Journal of Solid State Electrochemistry
https://doi.org/10.1007/s10008-019-04449-5

ORIGINAL PAPER

One-step electrochemical synthesis of MoS_2/graphene composite for supercapacitor application

Gomaa A. M. Ali[1,2] · Mohammad R. Thalji[1] · Wee Chen Soh[1] · H. Algarni[3,4] · Kwok Feng Chong[1]

Received: 14 June 2019 / Revised: 13 November 2019 / Accepted: 14 November 2019

Abstract

In this study, an MoS_2/graphene composite is fabricated from bulk MoS_2 and graphite rod via a facile electrochemical exfoliation method. The as-prepared samples are characterized by X-ray diffraction, field emission scanning electron microscopy, Fourier transform infrared spectroscopy and ultraviolet-visible spectroscopy techniques to confirm the formation of the MoS_2/graphene composite. The electrochemical behavior of the MoS_2/graphene composite is evaluated through cyclic voltammetry, galvanostatic charge/discharge and electrochemical impedance spectroscopy. It exhibits high specific capacitance of 227 F g^{-1} as compared with the exfoliated graphene (85 F g^{-1}) and exfoliated MoS_2 (70 F g^{-1}) at a current density of 0.1 A g^{-1}. This can be attributed to the synergistic effect between graphene and MoS_2. Moreover, it displays high electrochemical stability and low electrical resistance.

Keywords Electrochemical exfoliation · Supercapacitors · Graphene · Exfoliated MoS_2 · 2D materials

Introduction

Two-dimensional (2D) materials, such as graphene, have garnered great interest from researchers for decades due to their outstanding mechanical, optical and physical properties [1–3]. Besides graphene, transition metal dichalcogenides, particularly molybdenum disulfide (MoS_2), show promising potential in a wide range of applications including as catalysts and for energy storage and electronics [4, 5]. Bulk MoS_2 crystals can undergo exfoliation to form MoS_2 (a single, covalently bonded S–Mo–S tri-layer). This is the top-down synthesis approach for MoS_2. To date, various exfoliation approaches including sonication, ion intercalation and electrochemical exfoliation have been used to produce high-quality MoS_2 [6].

MoS_2 is a semiconducting compound that consists of a 2D plane of a hexagonal crystal structure which is analogous to graphene [7, 8]. Each MoS_2 layer consists of planes wherein the S–Mo–S atoms are combined by covalent bonds, and their neighboring layers are then attached to each other by weak van der Waals forces [9, 10]. From the other point of view, each Mo atom occupies a trigonal prism shape which is bound to six S atoms. The layered structure of MoS_2 provides a good platform for ion adsorption and diffusion, rendering it a great choice for supercapacitor applications [11]. On the other hand, another layered structure material, graphene, also possesses excellent physical properties for good energy storage applications [12, 13]. However, the major concern for layered structure material is the tendency for restacking of sheets to occur, which has a detrimental effect on the energy storage capacity. In this context, the proposal for utilizing two different layered structure materials is worth investigating, as the different

Highlights
- An MoS_2/graphene composite is obtained via one-step electrochemical exfoliation.
- The MoS_2/graphene composite is employed as electrode material for supercapacitor application.
- MoS_2/graphene shows high specific capacitance of 227 F g^{-1} (threefold > MoS_2 and graphene).
- MoS_2/graphene shows high electrochemical stability and low electrical resistance.

Electronic supplementary material The online version of this article (https://doi.org/10.1007/s10008-019-04449-5) contains supplementary material, which is available to authorized users.

✉ Kwok Feng Chong
ckfeng@ump.edu.my

[1] Faculty of Industrial Sciences & Technology, Universiti Malaysia Pahang, 26300 Kuantan, Malaysia

[2] Chemistry Department, Faculty of Science, Al-Azhar University, Assiut 71524, Egypt

[3] Research Centre for Advanced Materials Science (RCAMS), King Khalid University, P. O. Box 9004, Abha 61413, Saudi Arabia

[4] Department of Physics, Faculty of Sciences, King Khalid University, P. O. Box 9004, Abha, Saudi Arabia

Published online: 26 November 2019

surface properties of two different materials could prevent surface interaction.

Herein, we report a novel electrode material, MoS_2/graphene composite, for supercapacitor application. The MoS_2/graphene composite is prepared via a facile electrochemical approach from the co-electrochemical exfoliation of MoS_2 crystals and graphite rod. Interestingly, the incorporation of MoS_2 with graphene leads to a remarkable enhancement in the specific capacitance of the electrode, with high cycling stability and low electrical resistance.

Experimental techniques

Sample preparation

MoS_2, graphene and MoS_2/graphene composite were synthesized using an electrochemical exfoliation method as previously reported, with some modifications [14, 15]. The bulk MoS_2 crystal (99.99% purity, 429ML-AB, with size of 20 × 10 mm, SPI Supplies) was used as an anode, while a platinum wire was used as a cathode, with working distance of 2 cm in 1 M Na_2SO_4 solution. The preconditioning was conducted at DC voltage of 2 V for 5 min, followed by electrochemical exfoliation at 10 V for 5 min to obtain MoS_2. A similar process was employed by replacing the MoS_2 crystal with graphite rod (99.99% purity, 150 mm in length and diameter of 3 mm, Sigma-Aldrich) to exfoliate the graphite into graphene. Subsequently, a MoS_2/graphene composite was obtained by connecting the MoS_2 crystal and graphite rod as the anode using similar electrochemical conditions. Finally, exfoliated suspensions of MoS_2, graphene and MoS_2/graphene composite were collected separately using a polytetrafluoroethylene (PTFE) membrane (0.45 μm) and then washed with deionized water via vacuum filtration to remove the Na_2SO_4 solution. The collected samples were dried at 50 °C overnight in a vacuum oven.

Structural and morphological characterization

The crystal structure was analyzed using a Rigaku X-ray diffractometer (Miniflex II with Cu-K_α radiation at 40 kV, 30 mA, $\lambda = 1.5406$ Å) within the 2θ range of 5° to 80° at a scanning rate of 0.02 θ/s with a step time of 2 s. The functional groups were examined using a PerkinElmer (Spectrum 100) infrared spectrophotometer over the range of 400–4000 cm^{-1}. UV-Vis measurements were performed using a Thermo Scientific (Genesys 10S) UV spectrophotometer at room temperature. The surface morphological analysis was conducted using a JEOL (JSM-7800F) field emission scanning electron microscope (FESEM) coupled with energy-dispersive X-ray spectroscopy (EDX).

Electrochemical characterization

Working electrodes were prepared by pressing a slurry of MoS_2 or graphene or MoS_2/graphene composite (90 wt%), carbon black (5 wt%) and polyvinylidene fluoride (PVDF, 5 wt%) onto a piece of nickel foam, and then drying at 70 °C for 24 h. The final mass loading of the active materials per electrode was 3–4 mg. The electrochemical performance of the electrode was investigated using a three-electrode system (3-ES), which consists of the active material as the working electrode, Ag/AgCl (CH Instruments) as a reference electrode, and Pt wire (CH Instruments) as the counter electrode. The electrochemical data were collected using an electrochemical workstation (AUTOLAB PGSTAT30, Netherlands) equipped with a frequency response analyzer. Cyclic voltammetry (CV) tests were performed in the potential range of −0.8 to 0.2 V at different scan rates. Galvanostatic charge-discharge (GCD) tests were performed at different current densities. Electrochemical impedance spectroscopy (EIS) data were collected from 50 kHz to 0.01 Hz at open-circuit potential (OCP) with a voltage signal of 10 mV amplitude. All measurements were carried out in 1.0 M Na_2SO_4 electrolyte at room temperature.

Results and discussion

Structural and morphological characterization

Figure 1 shows the XRD patterns of graphene, MoS_2 and MoS_2/graphene composite. A sharp peak can be seen at 26.38° and another small peak at 43.24°, which are related to the (002) and (100) planes of the graphene structure, respectively. The (002) plane of graphite can be detected in graphene due to the multiple layers of graphene that are formed [16]. Electrochemical exfoliation of the layered structure involves driving ionic species (H_2O and SO_4^{2-}) at high potential to intercalate into the interlayer distance, locally forming gas bubbles (SO_2 and O_2) that force the adjacent sheets to separate [17]. Furthermore, the absence of a graphene oxide peak at 2θ ~14° also signifies a negligible amount of oxidation in the samples [17]. On the other hand, all marked peaks related to the MoS_2 have been indexed to the hexagonal phase of MoS_2 (JCPDS no. 37-1492). The MoS_2 pattern shows a sharp and visible peak at $2\theta = 14°$, which can be assigned to the (002) plane with d-spacing of 6.3 Å. This indicates the layered structure of MoS_2 along the c axis [18]. It can be seen that the MoS_2/graphene composite retains a layered crystallinity and the positions of diffraction peaks of MoS_2. However, it is worth noting that the intensity of the diffraction peaks of MoS_2 decrease with the incorporation of graphene, particularly the (002) peak. This indicates that the incorporation of graphene further restrains the stacking of

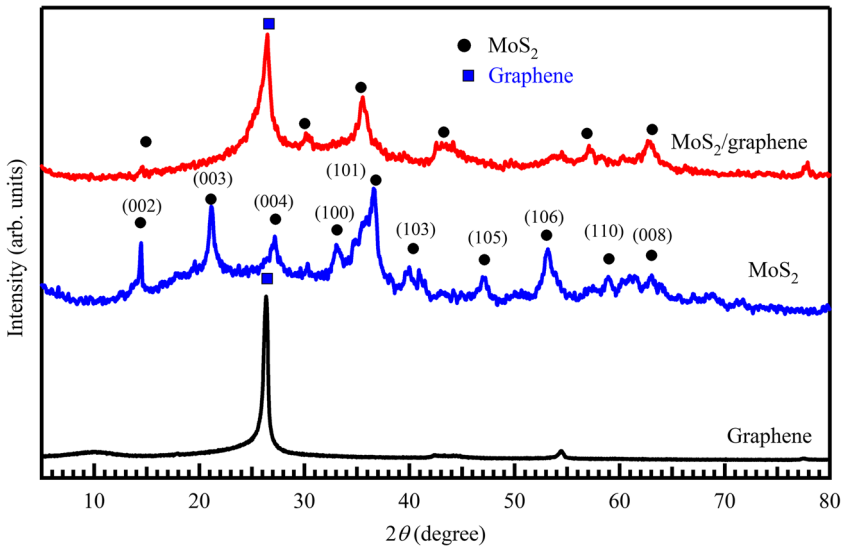

Fig. 1 XRD patterns of the graphene, MoS_2 and MoS_2/graphene composite

MoS_2 layers [19]. Furthermore, the presence of the graphene peak at 26.38° corresponding to the (002) plane is evidence that the graphene is incorporated into the composite.

Fourier transform infrared spectroscopy (FTIR) is employed to elucidate the functional groups of graphene, MoS_2 and the MoS_2/graphene composite [20]. As shown in Fig. 2, the peak at 620 cm^{-1} can be attributed to the Mo–S stretching vibration [21]. The multiple peaks at 700–1150 cm^{-1} can be assigned to the sulfate groups, while the sharp peaks at 3440 and 1610 cm^{-1} can be ascribed to the O–H stretching and water bending, respectively [22, 23]. This confirms the presence of sulfate and water molecules as intercalants during the electrochemical exfoliation process [24]. For the graphene spectrum, the intense peak located at 1610 cm^{-1} can be attributed to the aromatic C=C (stretching), and the very weak peak located at 1124 cm^{-1} corresponds to the C–O stretching [25]. In contrast, the absence of a C=O peak around 1715 cm^{-1} indicates the insignificant amount of oxidation of graphene. This further supports the XRD pattern of graphene, where the peak for graphene oxide (GO) is missing in the pattern. Interestingly, the intercalant-related peaks decrease in intensity for MoS_2/graphene composite, which indicates the intercalants are removed from the interlayer structure due to the difference in surface chemistry between graphene and MoS_2.

Figure 3a shows the UV-Vis spectra for MoS_2, graphene and MoS_2/graphene composite. Graphene exhibits a π-π* absorption band at 270 nm, which is in agreement with previous studies [26]. The results show that with the incorporation of graphene into MoS_2, the absorption band at 270 nm of the MoS_2/graphene composite increases. This phenomenon could be attributed to the black-body properties of graphene, which has been reported in the literature [27]. Figure 3b–c shows the relation between $(\alpha h\upsilon)^2$ and $h\upsilon$. The absorption coefficient (α) was calculated as $\alpha = 2.303 \times 10^{-3} A\rho/lC$, where A is the measured absorbance, ρ is the density, l is the optical path

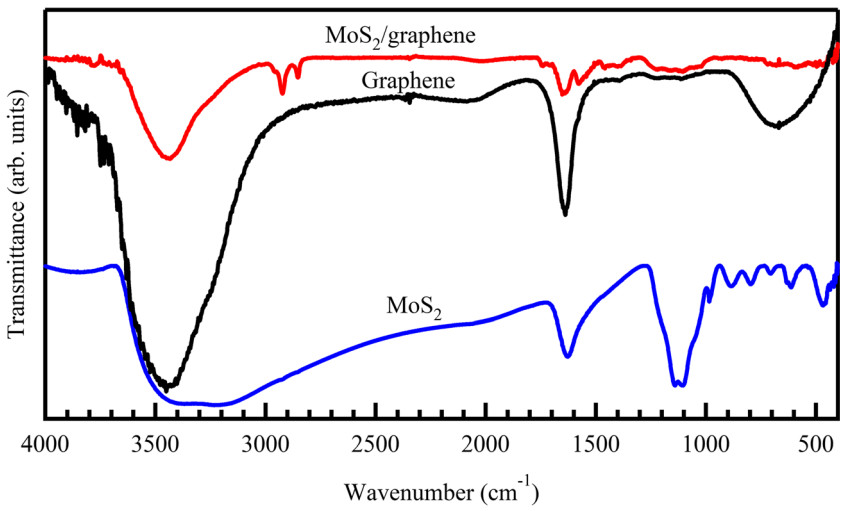

Fig. 2 FTIR spectra of MoS_2, graphene and MoS_2/graphene composite

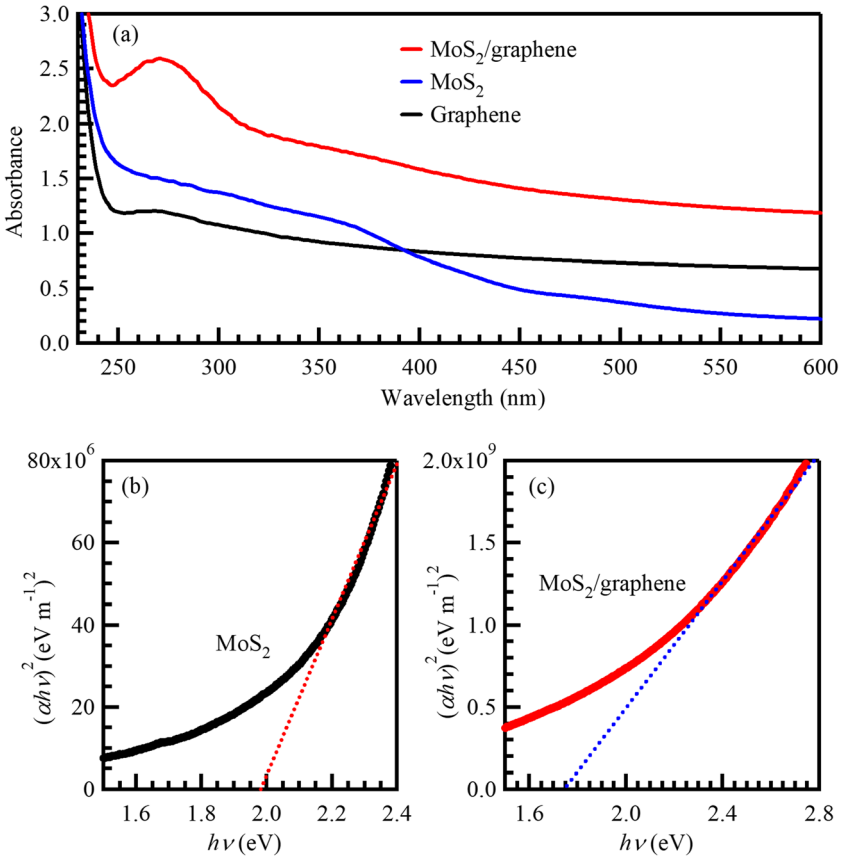

Fig. 3 UV-Vis spectra of the MoS_2, graphene and MoS_2/graphene composite (**a**), direct transition $((\alpha h\upsilon)^2$ vs. $h\upsilon)$ curves for MoS_2 (**b**) and MoS_2/graphene composite (**c**)

length and C is the concentration [8, 28]. Extrapolation of the linear portion to zero absorption coefficient gives the value of the optical energy gap, which is found to be 1.98 and 1.75 eV for MoS_2 and the MoS_2/graphene composite, respectively, suggesting direct electronic transitions which are in good agreement with the MoS_2 band structure. In addition, the bandgap value is closer to the reported values for monolayer MoS_2 (1.9 eV) than bulk MoS_2 (1.2 eV) [29], indicating the

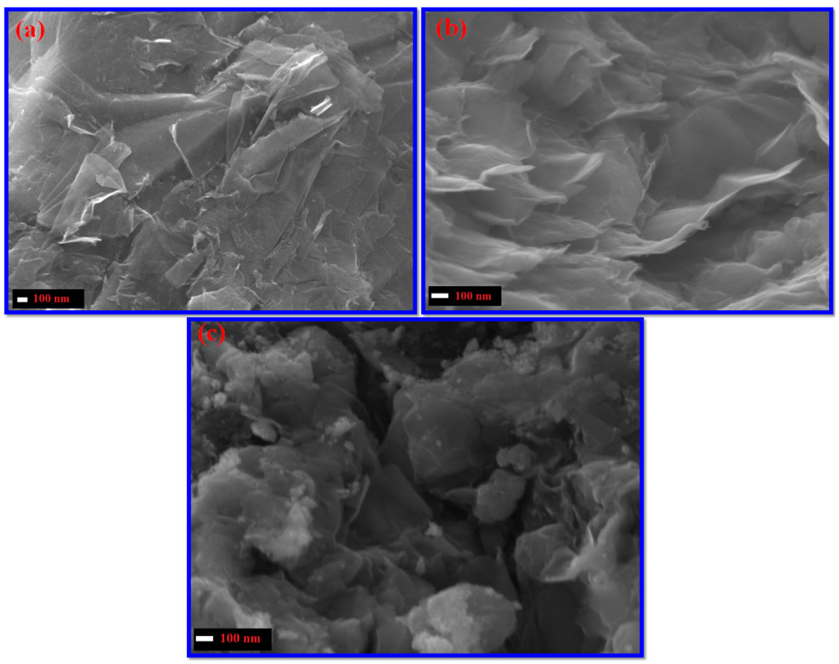

Fig. 4 FESEM images of MoS_2 (**a**), graphene (**b**) and MoS_2/graphene composite (**c**)

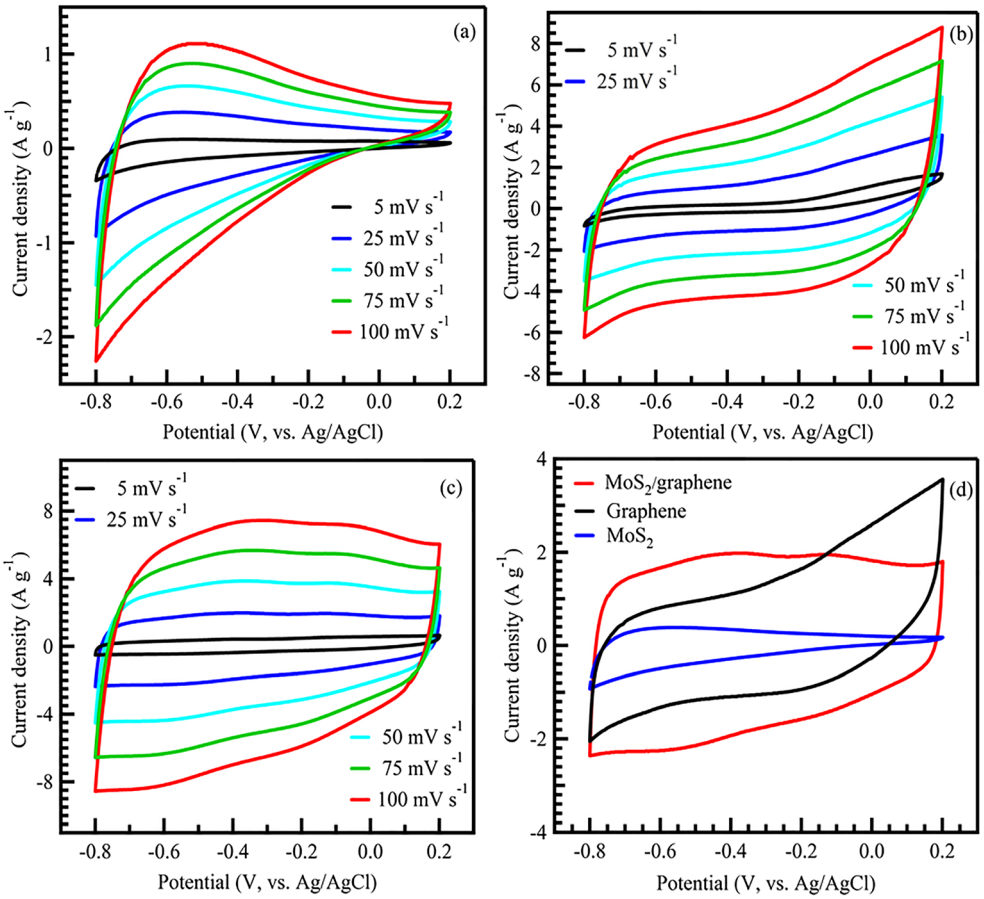

Fig. 5 Cyclic voltammetry curves of MoS_2 (**a**), graphene (**b**), MoS_2/graphene composite (**c**) at different scan rates and all as-prepared materials at 25 mV s^{-1} (**d**)

successful exfoliation of bulk MoS_2. Moreover, incorporation of MoS_2 with graphene leads to a decrease in the bandgap as a result of enhanced electrical conductivity of the hybrid material [30].

To reveal the morphology of all samples, FESEM analysis was employed. As illustrated in Fig. 4a and b, the FESEM images of MoS_2 and graphene show nanosheet formation. The close-up view of MoS_2/graphene composite in Fig. 4c shows the incorporation of MoS_2 nanosheets onto the graphene nanosheets. It is clear that the MoS_2 and graphene nanosheets are entwined to form an interconnected conductive network with a relatively smooth surface, which ensures optimum accessibility of electrolyte ions. Moreover, the elemental analysis for MoS_2/

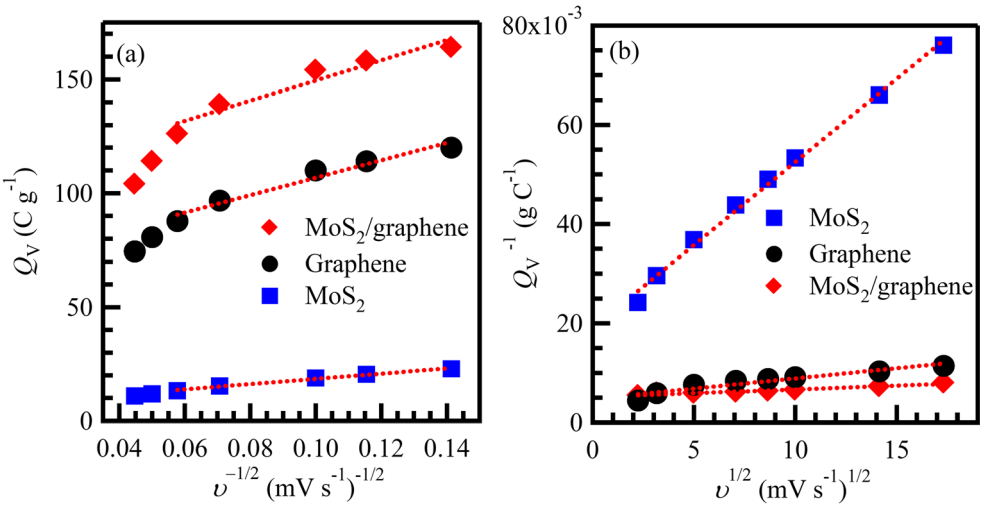

Fig. 6 Trasatti's analysis plots of Q_V vs. $\upsilon^{-1/2}$ (**a**) and Q_V^{-1} vs. $\upsilon^{1/2}$ (**b**) for MoS_2, graphene and MoS_2/graphene composite

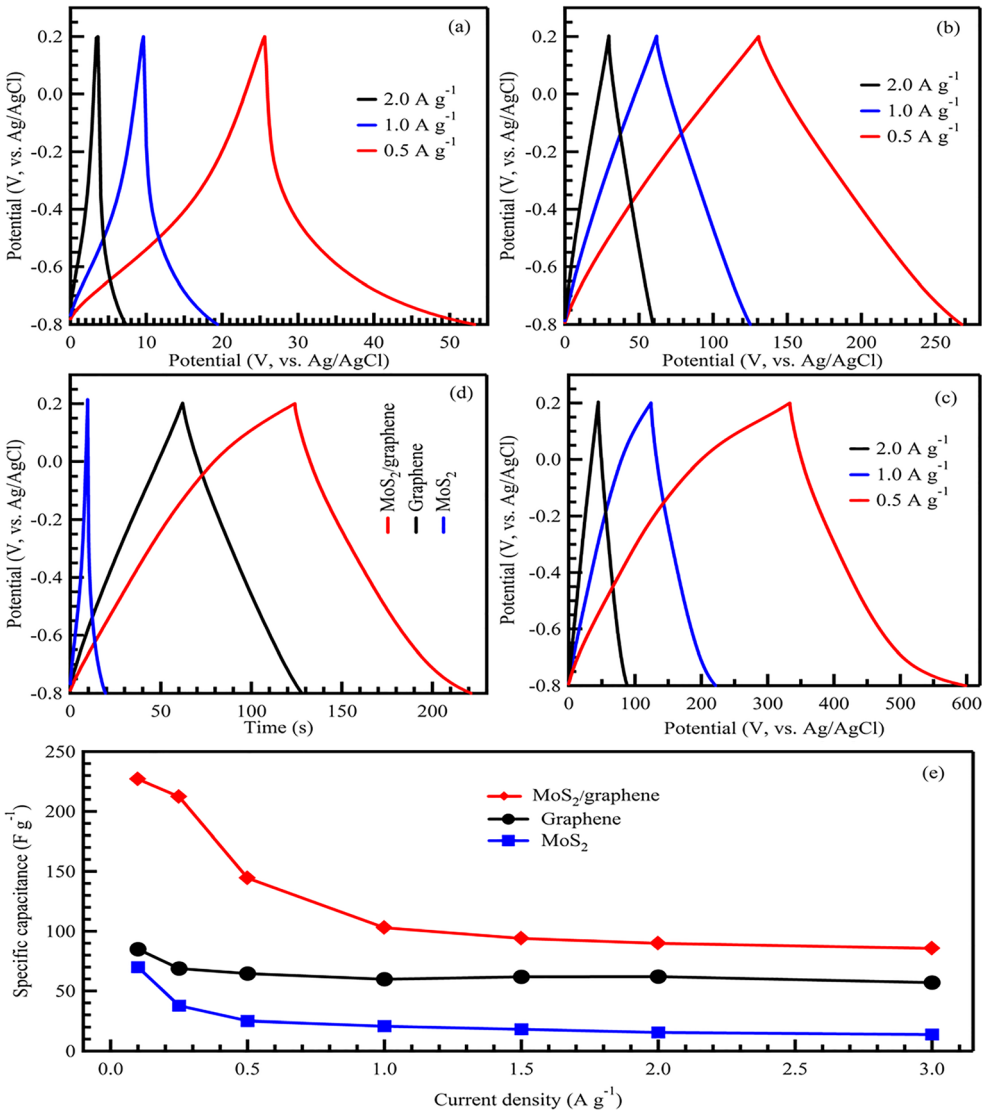

Fig. 7 GCD curves of MoS_2 (**a**), graphene (**b**), MoS_2/graphene composite (**c**) at current densities of 0.5, 1.0 and 2.0 A g^{-1}, GCD curves of all as-prepared materials at 1 A g^{-1} (**d**) and specific capacitance as a function of current density (**e**) for the indicated materials

graphene composite shows an atomic percent of 63.3, 14.5, 0.53 and 1.38% for C, O, Mo and S, respectively (Fig. S1). As we observed from FTIR findings, the oxygen content from EDX results could be related to the intercalated water molecule and sulfate ions. Overall, all of the results from XRD, FTIR, UV-Vis and FESEM confirm the successful electrochemical exfoliation to form MoS_2/graphene composite.

Electrochemical characterization

Cyclic voltammetry is performed to determine the electrochemical performance of samples using a three-electrode system under a potential window from −0.8 to 0.2 V at different scan rates. Based on the XRD results, the *d*-spacing of the interlayer MoS_2 structure is 6.3 Å. This is beneficial for rapid intercalation of hydrated Na^+ ions (hydrated ionic radius of the $Na(H_2O)_6^+$ is 2.43 Å) into MoS_2 layers [31]. As shown in Fig. 5a, the charge storage occurs mainly by the insertion/extraction of Na^+ ions into the interlayer of MoS_2, which can be seen from the oxidation peak at around 0.55 V. Similar pseudocapacitance of ion insertion/extraction was observed for MoS_2 in previous reports [32]. On the other hand, CV curves for graphene show an almost rectangular shape without any obvious redox peaks, which indicates the electrical double capacitance as the dominant charge storage mechanism (Fig. 5b). The slight deviation from the ideal rectangular shape may be due to the internal resistance or surface impurities. Figure 5c shows the CV curves of the MoS_2/graphene composite at different scan rates. The CV curves feature strong electrical double-layer capacitance with a near-rectangular shape, as well as pseudocapacitance with reversible redox peaks. It is evident that the electrical double-layer capacitance is contributed by graphene, while the pseudocapacitance is associated with the surface redox of MoS_2. Such synergistic effects between MoS_2 (faradaic

Table 1 Comparison of the specific capacitance and cycling stability with some previously reported studies for MoS_2 and graphene-based nanocomposites

Material	Specific capacitance (F g^{-1})	Stability (%)	Reference
Graphene-ZnO nanocomposites	196 @ 0.8 mA cm^{-2}	94.0 @ 5000 cycles	[37]
Graphene/VOx-NTs	210 @ 1 A g^{-1}	48.0 @ 5000 cycles	[38]
Graphene-honeycomb MnO_2	210 @ 0.5 A g^{-1}	82.4 @ 1000 cycles	[39]
Graphene oxide-MnO_2	216 @ 0.15 A g^{-1}	84.1 @ 1000 cycles	[40]
Fe_3O_4/graphene nanocomposites	220.1 @ 0.5 A g^{-1}	–	[41]
Multilayered graphene/MnO_2	252 @ 2 A g^{-1}	96.0 @ 6000 cycles	[42]
MoS_2-SnO_2	61.6 @ 1 A g^{-1}	90.0 @ 1000 cycles	[43]
MoS_2 @ 3D porous graphene	88.3 @ 0.1 A g^{-1}	78.0 @ 2000 cycles	[44]
MoS_2	144 @ 8×10^{-5} A g^{-1}	92.3 @ 1000 cycles	[45]
MoS_2/reduced graphene oxide	218.1 @ 1 A g^{-1}	91.8 @ 1000 cycles	[46]
MoS_2-graphene hybrid films	236 @ 8×10^{-5} A g^{-1}	92.5 @ 1000 cycles	[45]
h-rGO@MoS_2	238 @ 0.5 A g^{-1}	87.8 @ 3500 cycles	[47]
MoS_2/graphene	227 @ 0.1 A g^{-1}	89.0 @ 2000 cycles	This work

contribution) and graphene (non-faradaic contribution) can be represented by the following equations [32, 33]:

$$MoS_2 + xNa^+ + xe^- \leftrightarrow Na_xMoS_2 \quad (faradaic)$$
$$(MoS_2)_{surface} + xNa^+ + xe^- \leftrightarrow \left(Na^+ - MoS_2^-\right)_{surface} \quad (non-faradaic)$$

Furthermore, the CV curves retain their shape even at high scan rates, indicating the great high-rate performance. Noteworthily, the area of the CV curve for MoS_2/graphene composite is larger than that of MoS_2 and graphene at a scan rate of 25 mV s^{-1} (Fig. 5d), indicating that MoS_2/graphene composite displays improved capacitive behavior and high charge storage. Detailed charge storage calculation is studied under galvanostatic charge-discharge.

Trasatti's analysis method is utilized to provide insight with respect to the charge storage mechanism in MoS_2/graphene composite. Based on Equations (S1–S3) [34], the capacitive charge storage (Q_C) can be obtained as an intercept by extrapolating the plot of voltammetric charge (Q_V) vs. $\upsilon^{-1/2}$, and the total amount of stored charges (Q_T) is obtained as intercept (υ approaching 0) through extrapolation of the plot $1/Q_V$ vs. $\upsilon^{1/2}$. As a result, the Q_C value of MoS_2/graphene composite is measured to be 104.6 C g^{-1}, and it is higher than of the graphene and MoS_2, which are 68.8 and 6.5 C g^{-1}, respectively (Fig. 6a). The high Q_C value of MoS_2/graphene composite can be related to the improved electrical double-layer capacitance, probably due to the better ion accessibility within MoS_2/graphene structure. On the other hand, the Q_T value for MoS_2/graphene composite is 208.3 C g^{-1}, which is higher than that of graphene and MoS_2 (Table S1). It can be clearly seen that the charge storage in the MoS_2/graphene composite originates equally from the capacitive and diffusion contributions (50.2% and 49.8%, respectively), which confirms the synergistic effect between graphene and MoS_2.

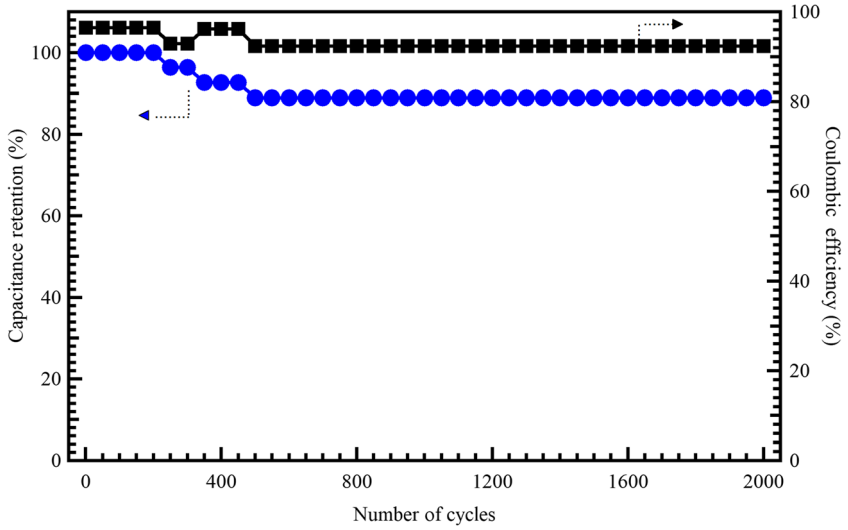

Fig. 8 Cycle life stability (left vs. bottom) and coulombic efficiency (right vs. bottom) at 1 A g^{-1} current density for MoS_2/graphene composite

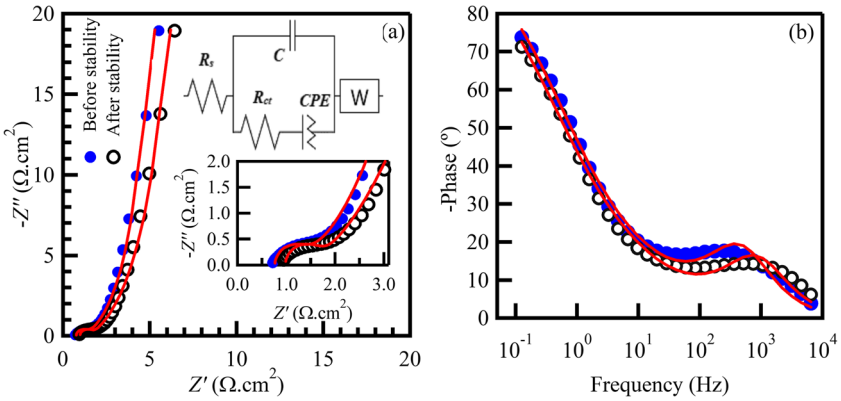

Fig. 9 Nyquist plots (with the insets of the high-frequency region and the equivalent circuit model) (**a**), Bode plots (**b**) for MoS_2/graphene composite electrodes before and after GCD stability

The electrochemical performance of MoS_2, graphene and MoS_2/graphene composite is further confirmed by GCD study at different current densities, as represented in Fig. 7a–c, respectively. The charging curves are symmetrical and linear to their discharge counterpart, which indicates the excellent reversibility of the samples. The discharge time significantly increases in MoS_2/graphene composite, indicating the increase in charge storage. Figure 7d compares the GCD curves of MoS_2, graphene and MoS_2/graphene electrodes at the current density of 1 A g^{-1}. It is worth noting that the MoS_2/graphene electrode has longer discharging time, indicating the higher specific capacitance of MoS_2/graphene than that of MoS_2 and graphene. The specific capacitance (C_{sp}) in F g^{-1} of the as-prepared electrodes was calculated as: $C_{sp} = I/m\left(\frac{dV}{dt}\right)$, where I is the discharge current, dV/dt is the slope of the discharge curve and m is the mass of active materials on the working electrode [11, 35, 36]. Based on Fig. 7e, MoS_2/graphene composite exhibits the highest specific capacitance of 227 F g^{-1} followed by low specific capacitance values of graphene (85 F g^{-1}) and MoS_2 (70 F g^{-1}) at a current density of 0.1 A g^{-1}. Despite the decrease in the specific capacitance with increasing current density, the MoS_2/graphene composite electrode still retains its higher capacitance as compared with other electrode materials at 5 A g^{-1}, indicating an excellent rate performance of MoS_2/graphene. A detailed comparison of specific capacitance reported with MoS_2 and graphene-based nanocomposites is listed in Table 1.

The cycling stability performance of MoS_2/graphene composite was determined by repeating the GCD test between −0.8 and 0.2 V at a current density of 1 A g^{-1} for 2000 cycles. The MoS_2/graphene electrode loss is only 11% from the initial specific capacitance, with high coulombic efficiency (93%). The high stability of the MoS_2/graphene composite is compared with related materials in Table 1. As shown in Fig. 8, the capacitance drop during the initial 250 cycles might be a result of the volume change due to electrolyte ion insertion. This phenomenon is widely seen in 2D materials [48].

To obtain further understanding of the electrochemical behavior of MoS_2/graphene electrode, EIS results were collected in a frequency range from 50 kHz to 0.1 Hz at OCP. The Nyquist plots (Fig. 9a) show two distinct parts, with a semicircle in the high-frequency region and a linear portion in the low-frequency region. The circuit fitting parameters are tabulated in Table 2. The equivalent circuit consists of a solution resistance (R_S), charge transfer resistance (R_{CT}), capacitor (C), constant phase element (CPE) and Warburg element (W). It shows that the MoS_2/graphene composite electrode possesses small values of R_S (0.76 Ω.cm^2) and R_{CT} (0.65 Ω.cm^2) as compared with graphene and MoS_2 electrodes (Fig. S2 and Table S2). The low resistance values are beneficial, as they are responsible for the quick charge transfer and fast ion diffusion to enhance electrochemical performance. The dependence of the phase angle on the frequency is evaluated in the Bode plot as presented in Fig. 9b, where the ideal capacitor behavior is represented by the phase shift of −90° in the low-frequency region [49]. The MoS_2/graphene composite electrode exhibits good capacitive performance (~ −75°), close to the ideal capacitor.

Table 2 The calculated parameters obtained by fitting of the experimental impedance data before and after the stability test for the MoS_2/graphene composite electrode

	R_S (Ω cm^2)	R_{CT} (Ω cm^2)	C (mF)	CPE (mF)	W (Ω cm^2)	S_E (cm^2 g^{-1})	τ (s)
Before stability	0.76	0.65	0.64	96.49	0.15	280.16	0.9
After stability	0.98	0.69	0.33	102.43	0.13	280.26	1.3

Moreover, the relaxation time ($\tau = 1/f^*$) can be obtained from the frequency at a phase angle of −45° [50], to give more information regarding the frequency response of the electrode material. As shown in Fig. 9b, the MoS_2/graphene composite electrode exhibits a frequency of 1.103 Hz, which corresponds to a time constant of 0.9 s. The small relaxation time indicates that the MoS_2/graphene composite electrode can switch more rapidly from resistive to capacitive behavior. To investigate the electrochemical stability of the electrode material, the EIS test was employed after GCD stability, as shown in the inset in Fig. 9a. The R_S and R_{CT} values increase slightly after the GCD stability test, demonstrating the excellent electrochemical stability of the MoS_2/graphene electrode [49].

Conclusions

In summary, a MoS_2/graphene composite was produced by a facile electrochemical approach. The synergistic effect between MoS_2 and graphene enhanced the charge storage of MoS_2/graphene to yield high specific capacitance of 227 F g^{-1}, which is higher than that of graphene (85 F g^{-1}) and MoS_2 (70 F g^{-1}). In addition, the MoS_2/graphene composite showed a long cycle life (89% after 2000 cycles) and low electrical resistance. These findings suggest that MoS_2/graphene could be a potential electrode for high-performance supercapacitors.

Acknowledgments The authors would like to acknowledge the funding from the Ministry of Education Malaysia in the form of FRGS [RDU1901186: FRGS/1/2019/STG07/UMP/02/6] and Universiti Malaysia Pahang grant RDU170357. Moreover, the authors extend their appreciation to King Khalid University, the Ministry of Education–Kingdom of Saudi Arabia for supporting this research through a grant (RCAMS/KKU/002-18) under the Research Center for Advanced Material Science. In addition, Dr. Gomaa A. M. Ali would like to express his thanks to SESAME Synchrotron (Allan, Jordan), which through the EU-funded project OPEN SESAME provided training on material characterization testing and data analysis.

Compliance with ethical standards

Conflict of interest The authors declare that they have no conflict of interest.

References

1. Quan Q, Lin X, Zhang N et al (2017) Graphene and its derivatives as versatile templates for materials synthesis and functional applications. Nanoscale 9:2398–2416
2. Lee SP, Ali GAM, Algarni H et al (2019) Flake size-dependent adsorption of graphene oxide aerogel. J Mol Liq 277:175–180
3. Wang J, Luo Q, Luo C et al (2017) High-performance supercapacitor electrode based on a nanocomposite of polyaniline and chemically exfoliated MoS_2 nanosheets. J Solid State Electrochem 21:2071–2077
4. Jia W, Tang B, Wu P (2018) Nafion-assisted exfoliation of MoS_2 in water phase and the application in quick-response NIR light controllable multi-shape memory membrane. Nano Res 11:542–553
5. Li Y, Wang H, Xie L et al (2011) MoS_2 nanoparticles grown on graphene: an advanced catalyst for the hydrogen evolution reaction. J Am Chem Soc 133:7296–7299
6. Tuteja SK, Duffield T, Neethirajan S (2017) Liquid exfoliation of 2D MoS_2 nanosheets and their utilization as a label-free electrochemical immunoassay for subclinical ketosis. Nanoscale 9:10886–10896
7. Ganatra R, Zhang Q (2014) Few-layer MoS_2: a promising layered semiconductor. ACS Nano 8:4074–4099
8. Aboelazm EAA, Ali GAM, Algarni H et al (2018) Flakes size-dependent optical and electrochemical properties of MoS_2. Curr Nanosci 14:416–420
9. Theerthagiri J, Senthil R, Senthilkumar B et al (2017) Recent advances in MoS_2 nanostructured materials for energy and environmental applications–a review. J Solid State Chem 252:43–71
10. Gusmão R, Sofer Z, Luxa J et al (2019) Antimony chalcogenide van der Waals nanostructures for energy conversion and storage. ACS Sustain Chem Eng 7:15790–15798
11. Zhang S, Song X, Liu S et al (2019) Template-assisted synthesized MoS_2/polyaniline hollow microsphere electrode for high performance supercapacitors. Electrochim Acta 312:1–10
12. Raccichini R, Varzi A, Passerini S et al (2015) The role of graphene for electrochemical energy storage. Nat Mater 14:271–279
13. Ali GAM, Makhlouf SA, Yusoff MM et al (2015) Structural and electrochemical characteristics of graphene nanosheets as supercapacitor electrodes. Rev Adv Mater Sci 40:35–43
14. Liu N, Kim P, Kim JH et al (2014) Large-area atomically thin MoS_2 nanosheets prepared using electrochemical exfoliation. ACS Nano 8:6902–6910
15. Ambrosi A, Pumera M (2018) Electrochemical exfoliation of MoS_2 crystal for hydrogen electrogeneration. Chem Eur J 24:18551–18555
16. Jia Y, Wan H, Chen L et al (2017) Hierarchical nanosheet-based MoS_2/graphene nanobelts with high electrochemical energy storage performance. J Power Sources 354:1–9
17. Achee TC, Sun W, Hope JT et al (2018) High-yield scalable graphene nanosheet production from compressed graphite using electrochemical exfoliation. Sci Rep 8:14525
18. Liu Y, Zhao Y, Jiao L et al (2014) A graphene-like MoS_2/graphene nanocomposite as a highperformance anode for lithium ion batteries. J Mater Chem A 2:13109–13115
19. Chen Y, Ma W, Cai K et al (2017) In situ growth of polypyrrole onto three-dimensional tubular MoS_2 as an advanced negative electrode material for supercapacitor. Electrochim Acta 246:615–624
20. Kee CW (2015) Assignment of O–O and Mo=O stretching frequencies of molybdenum/tungsten complexes revisited. J Chem 2015:439270–439279
21. da Silveira Firmiano EG, Rabelo AC, Dalmaschio CJ et al (2014) Supercapacitor electrodes obtained by directly bonding 2D MoS_2 on reduced graphene oxide. Adv Energy Mater 4:1301380–1301387
22. Zhou K, Jiang S, Bao C et al (2012) Preparation of poly(vinyl alcohol) nanocomposites with molybdenum disulfide (MoS_2): structural characteristics and markedly enhanced properties. RSC Adv 2:11695–11703
23. Teo EYL, Ali GAM, Algarni H et al (2019) One-step production of pyrene-1-boronic acid functionalized graphene for dopamine detection. Mater Chem Phys 231:286–291

24. Liu H, Chen B, Liao L et al (2019) The influences of mg intercalation on the structure and supercapacitive behaviors of MoS_2. J Mater Sci 54:13247–13254
25. Tanhaei M, Mahjoub AR, Safarifard V (2019) Energy-efficient sonochemical approach for the preparation of nanohybrid composites from graphene oxide and metal-organic framework. Inorg Chem Commun 102:185–191
26. Zhang R, Wan W, Li D et al (2017) Three-dimensional MoS_2/reduced graphene oxide aerogel as a macroscopic visible-light photocatalyst. Chin J Catal 38:313–320
27. Zhou Y, Zhang X, Zhang Q et al (2014) Role of graphene on the band structure and interfacial interaction of Bi_2WO_6/graphene composites with enhanced photocatalytic oxidation of NO. J Mater Chem A 2:16623–16631
28. Ali GAM, Fouad OA, Makhlouf SA (2013) Structural, optical and electrical properties of sol–gel prepared mesoporous Co_3O_4/SiO_2 nanocomposites. J Alloys Compd 579:606–611
29. Wang Q, Huang J, Sun H et al (2018) MoS_2 quantum dots@TiO_2 nanotube arrays: an extended-spectrum-driven photocatalyst for solar hydrogen evolution. ChemSusChem 11:1708–1721
30. Abdi MM, Ekramul Mahmud HNM, Abdullah LC et al (2012) Optical band gap and conductivity measurements of polypyrrole-chitosan composite thin films. Chin J Polym Sci 30:93–100
31. Li Z, Xiang K, Xing W et al (2015) Reversible aluminum-ion intercalation in prussian blue analogs and demonstration of a high-power aluminum-ion asymmetric capacitor. Adv Energy Mater 5: 1401410
32. Wang R, Wang S, Peng X et al (2017) Elucidating the intercalation pseudocapacitance mechanism of MoS_2–carbon monolayer interoverlapped superstructure: toward high-performance sodium-ion-based hybrid supercapacitor. ACS Appl Mater Interfaces 9: 32745–32755
33. Sarkar D, Das D, Das S et al (2019) Expanding interlayer spacing in MoS_2 for realizing an advanced supercapacitor. ACS Energy Letters 4:1602–1609
34. Thalji MR, Ali GAM, Algarni H et al (2019) Al^{3+} ion intercalation pseudocapacitance study of $W_{18}O_{49}$ nanostructure. J Power Sources 438:227028
35. Aboelazm EAA, Ali GAM, Chong KF (2018) Cobalt oxide supercapacitor electrode recovered from spent lithium-ion battery. Chem Adv Mater 3:67–74
36. Ali GAM, Fouad OA, Makhlouf SA et al (2014) Co_3O_4/SiO_2 nanocomposites for supercapacitor application. J Solid State Electrochem 18:2505–2512
37. Li Z, Zhou Z, Yun G et al (2013) High-performance solid-state supercapacitors based on graphene-ZnO hybrid nanocomposites. Nanoscale Res Lett 8:473
38. Fu M, Ge C, Hou Z et al (2013) Graphene/vanadium oxide nanotubes composite as electrode material for electrochemical capacitors. Phys B Condens Matter 421:77–82
39. Zhu J, He J (2012) Facile synthesis of graphene-wrapped honeycomb MnO_2 nanospheres and their application in supercapacitors. ACS Appl Mater Interfaces 4:1770–1776
40. Chen S, Zhu J, Wu X et al (2010) Graphene oxide-MnO_2 nanocomposites for supercapacitors. ACS Nano 4:2822–2830
41. Wang Q, Jiao L, Du H et al (2014) Fe_3O_4 nanoparticles grown on graphene as advanced electrode materials for supercapacitors. J Power Sources 245:101–106
42. Wu M-S, Lin C-J, Ho C-L (2012) Multilayered architecture of graphene nanosheets and MnO_2 nanowires as an electrode material for high-performance supercapacitors. Electrochim Acta 81:44–48
43. Prabukumar C, Mohamed Jaffer Sadiq M, Krishna Bhat D et al (2019) SnO_2 nanoparticles functionalized MoS_2 nanosheets as the electrode material for supercapacitor applications. Mater Res Express 6:085526
44. Zhang F, Tang Y, Liu H et al (2016) Uniform incorporation of flocculent molybdenum disulfide nanostructure into three-dimensional porous graphene as an anode for high-performance lithium ion batteries and hybrid supercapacitors. ACS Appl Mater Interfaces 8:4691–4699
45. Patil S, Harle A, Sathaye S et al (2014) Development of a novel method to grow mono−/few-layered MoS_2 films and MoS_2–graphene hybrid films for supercapacitor applications. CrystEngComm 16:10845–10855
46. Xiao W, Zhou W, Feng T et al (2016) Simple synthesis of molybdenum disulfide/reduced graphene oxide composite hollow microspheres as supercapacitor electrode material. Materials 9:783–796
47. Zheng S, Zheng L, Zhu Z et al (2018) MoS_2 nanosheet arrays rooted on hollow rGO spheres as bifunctional hydrogen evolution catalyst and supercapacitor electrode. Nano-Micro Lett 10:62–72
48. Wang J, Wu Z, Hu K et al (2015) High conductivity graphene-like MoS_2/polyaniline nanocomposites and its application in supercapacitor. J Alloys Compd 619:38–43
49. Ali GAM, Manaf SAA, Divyashree A et al (2016) Superior supercapacitive performance in porous nanocarbons. J Energy Chem 25:734–739
50. Ali GAM, Yusoff MM, Shaaban ER et al (2017) High performance MnO_2 nanoflower supercapacitor electrode by electrochemical recycling of spent batteries. Ceram Int 43:8440–8448